Polarization effects in the simulation of lead (II) fluoride



1999 J. Phys.: Condens. Matter 11 9009

(http://iopscience.iop.org/0953-8984/11/46/304)

J. Phys.: Condens. Matter **11** (1999) 9009–9024. Printed in the UK PII: S0953-8984(99)07903-5

# Polarization effects in the simulation of lead (II) fluoride

Michael J Castiglione, Mark Wilson and Paul A Madden

Physical and Theoretical Chemistry Laboratory, Oxford University, South Parks Road, Oxford OX1 3QZ, UK

Received 16 September 1999

**Abstract.** An interionic potential to describe the interactions in $PbF_2$ is constructed from *ab initio* calculations. The potential is based upon formal ionic charges and includes polarization effects arising from the induced dipoles on both anions and cations. The cation polarization effects are shown to be crucial to explain observable differences between $PbF_2$ and alkaline-earth fluorides of comparable cation size ($SrF_2$ and $BaF_2$). In particular, the lower transition pressure between the $\beta$- (fluorite) and $\alpha$- (cotunnite) phases and the qualitative difference between the shapes of the phonon dispersion for $PbF_2$ and the alkaline earths are reproduced. Simulations show a transition to a superionic conducting state in the $\beta$-phase, though at a temperature slightly higher than that observed experimentally. No ionic conduction is observed in the $\alpha$-phase at comparable temperatures, in agreement with experiment. The pattern of diffuse neutron scattering predicted by the simulations in the superionic domain is shown to reproduce the distinctive distribution of intensity observed experimentally.

## 1. Introduction

Lead fluoride is one of a number of systems of stoichiometry $MX_2$ which adopt the cubic fluorite crystal structure and which exhibit fast-ion conduction [1]. Of the halides in this class, it is the one exhibiting the lowest transition temperature to the conducting régime and, as such, has been extensively studied experimentally [2–4]. Related oxide systems include (cubic) zirconia and uranium dioxide, where the ionic conduction process has important technological implications [5, 6]. The focus of our present simulation work is on developing realistic simulation models, by appeal to first-principles calculations, so as to examine how the properties of the material are affected by the underlying chemistry. This relates not just to the mechanism of the ionic conduction process itself, but also to the stability of the fluorite structure relative to other phases which are not ionically conducting. In the case of $PbF_2$, a non-conducting cotunnite ($\alpha$-$PbCl_2$) phase is reached at a transition pressure of 0.5 GPa. Both the degree of ionic conduction and the stability of the cubic phase relative to other phases are affected by the addition of other binary compounds of different stoichiometry. In $PbF_2$, addition of KF has been shown to promote a large increase in ionic conduction and a reduction in the transition temperature [7]. The cubic phase of zirconia is stabilized by the addition of $Y_2O_3$ or CaO to produce highly conductive materials which act as oxide sensors. One reason for pursuing the goal of a 'realistic' simulation model is the hope that such potentials could be *transferred* to such mixtures, thereby permitting a reliable comparison of their properties with those of the parent material.

In order to illustrate the 'chemical' effects on the properties of $PbF_2$ it is instructive to compare with the alkaline-earth fluorides ($CaF_2$, $SrF_2$ and $BaF_2$), with which $PbF_2$ shares

0953-8984/99/469009+16$30.00  

broad similarities. Table 1 lists the lattice energy, superionic transition temperatures, melting temperatures and transition pressures for the transition from the fluorite $\beta$-form (eight-coordinate cations) to the cotunnite ($\alpha$-form $\equiv$ $\alpha$-$PbCl_2$, 7 + 2 coordinate cations) structure. In the simplest 'rigid-ion' model of the interactions, $PbF_2$ would be expected to exhibit similar behaviour to $SrF_2$ and $BaF_2$, since the $Pb^{2+}$ ionic radius is intermediate between those of $Sr^{2+}$ and $Ba^{2+}$ [8]. However, $PbF_2$ stands out as anomalous in that neither the superionic and melting temperatures nor the phase transition pressure fit the pattern of the alkaline-earth fluorides with increasing cation radius. Both the melting and superionic transition temperatures appear at significantly lower temperatures whilst the transition to the cotunnite structure occurs at a significantly lower pressure. Furthermore, whilst the experimental phonon dispersion curves for $CaF_2$, $SrF_2$ and $BaF_2$ [9–11] show very similar line shapes in the high-symmetry directions, the experimental $PbF_2$ phonon dispersion curves [3] appear 'anomalous' in that some modes are particularly soft. One factor which this rigid-ion picture does not allow for is the much greater polarizability of the $Pb^{2+}$ ion relative to the alkaline earths. This arises because the outer-electron configuration of the $Pb^{2+}$ ion is $6s^2$, with the result that low-energy dipole-allowed transitions to the 6p orbitals are possible. The refractive index indicates a large lead-cation polarizability [12] and this is confirmed by electronic structure calculations, which give $\alpha_{Pb^{2+}} = 17.9$ au [13] compared with $\alpha_{Sr^{2+}} = 5.2$ au [14]. Furthermore, the polarizability of the lead cation is significantly greater than that of the fluoride anion ($\alpha_{F^-} = 7.78$ au [13]). That SnO and PbO adopt relatively low-symmetry crystal structures (anti-litharge) compared to the alkaline-earth oxides has already been attributed to cation polarization [15, 16]. It is tempting, even at this early stage, to assign the anomalously low superionic transition temperature in $PbF_2$ to this greater cation polarizability. Indeed, previous work on $CaF_2$ has already shown how the inclusion of cation polarization effects does lower such transition temperatures by reducing the barrier heights for the activated diffusion processes [17] of the mobile $F^-$ ions. Similarly, the fact that the lattice energy is substantially larger than that of $SrF_2$ (which has a smaller lattice constant) could be due to a greater dispersion energy for the more polarizable cation.

**Table 1.** Comparison of a range of experimental properties for the fluorite structures for $PbF_2$ and three alkaline-earth halides.

| System | $\sigma_+$/Å | $a_0$/Å | $T_c$/K | $T_m$/K | $P_t$/GPa | $\Delta H_{latt}$ |
|---|---|---|---|---|---|---|
| $CaF_2$ | 0.99 | 5.45 | 1430 | 1696 | 10.0 | 2609.2 |
| $SrF_2$ | 1.13 | 5.78 | 1400 | 1723 | 6.0 | 2448.2 |
| $BaF_2$ | 1.35 | 6.18 | 1230 | 1550 | 5.0 | 2307.2 |
| $PbF_2$ | 1.20 | 5.92 | 711 | 1128 | 0.5 | 2487.2 |

In previous MD simulation work on $PbF_2$, empirically parametrized, 'rigid-ion' effective pair potentials have been used, in which polarization (and other, possible many-body) effects are subsumed within the effective interaction parameters. A consequence of this is that potential parameters acquire unphysical values if viewed as properties of true pair interactions; in particular, the 'dispersion' parameters $C_6$ for the F–F interactions in $CaF_2$ were found to be about six times greater than could be justified on an *ab initio* basis. This enhanced F–F attraction promoted $F^-$-ion disorder in the $CaF_2$ simulation, leading to superionic behaviour. In a realistic ionic potential, this effect appears to be attributable to the polarization effects. Although the effective pair potential appears to give quite good agreement with the experimental anion diffusion coefficients for the pure materials (for $PbF_2$ as well as $CaF_2$), other properties, such as the phonon dispersion curves, are less well predicted, and such potentials do not transfer well to related systems. We have already highlighted the significance of mixed-cation fluorite

systems technologically, and that studying them is one goal. Shell models, which contain an explicit representation of the polarization effects, have been developed for $PbF_2$, but these have proven unstable in MD simulations [18] due to the strong interactions of the induced dipoles on cations and anions in simulations at finite temperature. In this work we show how it is possible to overcome this technical challenge using the polarizable-ion methodology (PIM), described in full elsewhere [19].

The interaction model includes full, formal charges on the ions, and the $Pb^{2+}$ and $F^-$ ions have their full polarizabilities, as above. Wherever possible *ab initio* calculations are used to parametrize sections of the model unambiguously. In order to examine the factors affecting the observable properties, simulations have been performed with related models in which the polarization effects are omitted or enhanced. The simulation model is validated by comparison with experimental data on the lattice energy and volume (including their relationship for the fluorite and cotunnite structures), the phonon dispersion curves, and the ion mobility in the ionically conducting régime. We also compare the calculated coherent diffuse neutron scattering intensities with experiment: this observable directly probes the correlations on the disordered fluoride-ion sublattice and has been shown to exhibit different characteristic patterns for $PbF_2$ and $CaF_2$, suggesting that it may be a stringent test for the fluoride disorder in the simulated system. The mechanism of the ionic conduction in $PbF_2$, and its relationship to the disorder sensed in the diffuse scattering experiments, and the role of other cations in promoting ionic diffusion will be discussed elsewhere.

## 2. Constructing and testing the potential

The interaction model includes a pair potential, which incorporates short-range repulsion and dispersion, together with an account of the polarization effects which result from the induction of dipoles on both the $Pb^{2+}$ and $F^-$ ions. Note that in the perfect fluorite structure, all ions sit at sites of high symmetry, so dipole induction cannot contribute to the energetics, which is therefore fully determined by the pair potential in this representation.

### *2.1. An ab initio pair potential*

The procedure for generating an effective pair potential (EPP) is analogous to that previously used for $CaF_2$ [17]. Pyper has calculated repulsion and dispersion energies for $PbF_2$ in the perfect crystalline $\beta$-form (the fluorite) as a function of lattice parameter, $R$, using *ab initio* electronic structure methods [13]. The repulsive energy, $U^{rep}(R)$, due to cation–anion interactions, is expressed as the sum of two terms: a 'self-energy' (or 'rearrangement energy'), $U_a^{self}$, which is the energy required to compress the electron density of anion $a$ from that of a free ion into the crystal at lattice parameter $R$, and an 'overlap energy', $U_{ab}^{ov}(R)$, which is the energy of overlap of the anion electron density, compressed to the extent appropriate to lattice parameter $R$, with the cation electron density. An effective pair potential for the cation–anion interactions is constructed by combining these two terms:

$$4u_{+-}^{EPP}(R) = U_-^{self}(R) + 4U_{+-}^{ov}(R). \tag{2.1}$$

The factor of four arises from the anion–cation coordination in the fluorite crystal. Whilst it is possible to construct a model in which the integrity of the two terms is maintained (a compressible-ion mode, CIM [20]) the effect of the CIM is relatively small for bound ions such as $F^-$ [17] and so an EPP is preferred for simplicity. The consequences of this simplification will be noticed when we compare the energies of fluorite with cotunnite, which has a different

coordination number. A difference from the previous $CaF_2$ potential is that a potential of the form

$$u_{+-}^{EPP} = \frac{B_{ij}}{r_{ij}} e^{-a_{ij}r_{ij}} + B'_{ij} e^{-a'_{ij}r_{ij}^2} \tag{2.2}$$

is used to fit the *ab initio* data. In fact, as for $CaF_2$, a single exponential can be used to fit the complete *ab initio* data set over the lattice parameters available (down to 4 au). However, in the present work the cation polarizability is several times larger than that in $CaF_2$ (see the following section) which can lead to instability problems at very small anion–cation separations (considerably smaller than the normal lattice separation). The second exponential acts as a steep repulsive wall at separations for $R < 4a_0$. The $(B_{ij}/r_{ij})e^{-a_{ij}r_{ij}}$ form was chosen in preference to a standard $B_{ij}e^{-a_{ij}r_{ij}}$ potential since the former gave a better fit to the *ab initio* data. The fitted exponentials are shown in figure 1. The anion–anion and cation–cation potentials were derived from the same source and were fitted to single exponentials.

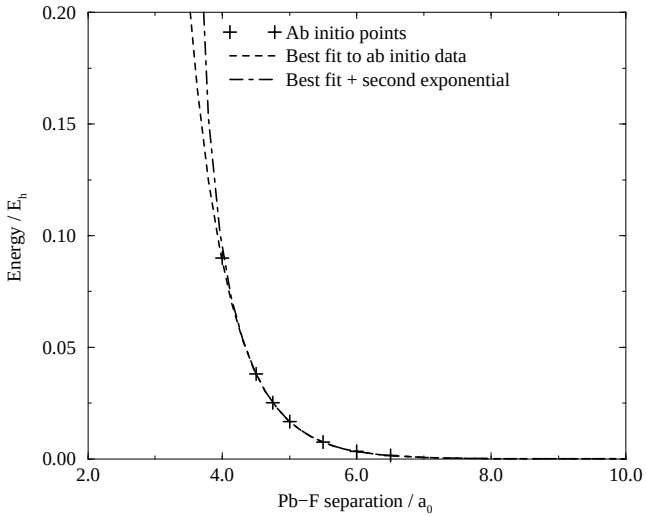


**Figure 1.** Two fits to the *ab initio* data points [13] are shown. The dashed curve shows the best fit to the data with a single exponential and the dot–dashed one the effect of adding a further steep repulsive term. This is seen to have no effect in the region of the $Pb^{2+}$–$F^-$ nearest-neighbour separation ($4.6a_0$).

The choice of the second exponential terms $B'_{+-}$ and $a'_{ij}$ is relatively less well controlled. The highly polarizable nature of the cation means that, at very short anion–cation separations, the attractive ion–dipole forces can still overwhelm even the $Be^{ar}/r$ term. The use of the second exponential term acts to prevent this by imposing a much harder repulsive wall at $r < 4a_0$. Since the shortest anion–cation separation considered in the *ab initio* data used to fit the above potential is $4a_0$, the choice of the additional terms is relatively free. As a result, we have chosen parameters which avoid the above instability whilst leaving unaffected such properties as those of the low-temperature phonons. It is, however, interesting to speculate as to the physical reasons behind the existence of such a relatively hard potential wall. A possible interpretation is that the $Pb^{2+}$ ion could be thought of as a $Pb^{4+}$ 'core' with an $s^2$ outer shell. In this picture the $s^2$ outer shell dominates the repulsive interactions at $r > 4a_0$ whilst the $Pb^{4+}$ core would dominate below this point. Indeed, analysis of the crystal structure of $PbF_4$ shows that the two shortest Pb–F distances in this system are of the order of $3.67a_0$ and $4.01a_0$ respectively [21], certainly consistent with the proposed hard wall just below $4a_0$.

The dispersion parts of the pair potential include the long-range $C_6 r^{-6}$ (dipole–dipole) and $C_8 r^{-8}$ (dipole–quadrupole) terms, with $r$-dependencies modified at short range to account for dispersion damping [22]. The dispersion parameters $C_6$ and $C_8$ are taken from Pyper [13] and are calculated from the in-crystal polarizabilities ($\alpha_{F^-} = 7.783$ au and $\alpha_{Pb^{2+}} = 17.9$ au respectively). Notably, the dispersion interactions for ion pairs involving $Pb^{2+}$ are much greater in magnitude than for $Ca^{2+}$ in $CaF_2$ [17]. Note too that the anion–anion dispersion parameter, at $34.372 E_h a_0^6$ is much smaller than that ($179.6 E_h a_0^6$) in the rigid-ion potential of Walker *et al* [23]. There is a clear analogy with the previous studies of $CaF_2$ [17], where an unphysically large anion–anion dispersion parameter is found in the rigid-ion potential which gives fast-ion conduction.

In our work, the dispersion damping is described by Tang–Toennies functions (as in [17]), which contain a single parameter which specifies the length scale on which the damping becomes effective. In the present work the $CaF_2$ parameters are used [17]. All potential parameters are given in table 2.

**Table 2.** Pair-potential parameters (equation (2.2)).

| Parameter | Anion–anion | Anion–cation | Cation–cation |
|---|---|---|---|
| $a$ | 2.788 | 1.435 | 2.1447 |
| $B$ | 2576.0 | 110.29 | 4613.6 |
| $a'$ | 0.0 | 1.0 | 0.0 |
| $B'$ | 0.0 | 50000 | 0.0 |
| $C_6$ | 34.372 | 53.045 | 91.858 |
| $C_8$ | 538.779 | 711.042 | 1022.752 |

### *2.2. Representation of the polarization effects*

In the current work only dipole polarization effects will be considered. In the perfect fluorite structure, used to parametrize the short-range potential, the ions lie in ideal tetrahedral or cube-centre sites and so no dipoles are induced. In the high-pressure $\alpha$-$PbF_2$ structure ($\equiv\alpha$-$PbCl_2$) the ions are in less symmetric (though high-coordination) environments and so a small contribution to the lattice energy from the induced dipoles is anticipated. *Ab initio* calculations on distorted crystals in which dipoles may be induced on the ions have shown that the total induced dipole can be usefully decomposed into two effects [24, 25]. Firstly, the electric field due to the ionic charges in the distorted crystal induces a 'Coulombic' dipole whose magnitude is governed by the in-crystal polarizabilities derived from electronic structure calculations ($\alpha_{F^-} = 7.783$ au and $\alpha_{Pb^{2+}} = 17.9$ au). Secondly, this dipole must be corrected for short-range effects which have been examined in electronic structure calculations for alkali halide systems [26].

To deal with these effects in the simulation, we include an explicit representation of the induced dipoles as variables, comparable to the ion positions, used to characterize the state of the system and its energy. The induced dipole on each ion, for a given configuration, is obtained by minimization of the potential

$$U_{pol} = \sum_{i=2}^{N} \sum_{j=i+1}^{N-1} (\boldsymbol{T}^{(1)}(\boldsymbol{r}_{ij}) f_{ij}(r_{ij})(q_j \boldsymbol{\mu}_i - q_i \boldsymbol{\mu}_j) + \boldsymbol{\mu}_i \cdot \boldsymbol{T}^{(2)}(\boldsymbol{r}_{ij}) \cdot \boldsymbol{\mu}_j) + \sum_i \frac{1}{2} k^i \mu_i^2 \qquad (2.3)$$

with respect to all the dipoles $\{\mu_i\}$. These self-consistent dipoles are the induced dipoles of the model and $U_{pol}$ evaluated with these dipoles is the polarization energy associated with that configuration. The final term in the equation is a Drude-like representation of the

energy required to polarize each ion and the force constant $k^i$ is determined by the ionic polarizability ($\alpha^i$):

$$k^i = \frac{1}{2\alpha^i}. \tag{2.4}$$

In equation (2.3), $q^i$ is the formal ionic charge, and the $\boldsymbol{T}^{(n)}$-tensors are the normal charge–dipole and dipole–dipole interaction tensors:

$$T_\alpha^{(1)}(\boldsymbol{r}) = -r_\alpha/r^3 \qquad T_{\alpha\beta}^{(2)}(\boldsymbol{r}) = (3r_\alpha r_\beta - r^2\delta_{\alpha\beta})/r^5. \tag{2.5}$$

The $r$-dependence of the charge–dipole interaction is modified to account for the short-range induction effects uncovered in the electronic structure calculations by the factor $f_{ij}(r_{ij})$, which depends on the identities of the ions involved and which is a function of their separation. A suitable form for this function has been found to be (as suggested by the Tang–Toennies dispersion 'damping' functions [27])

$$f_{ij}(r) = 1 - c_{ij}\left(\sum_{k=0}^{4}\frac{(b_{ij}r)^k}{k!}\right)\mathrm{e}^{-b_{ij}r}. \tag{2.6}$$

This function switches from the large-$r$ value of 1 (meaning that the charge–dipole interaction regains the pure Coulombic form in this limit) to $1 - c_{ij}$ at $r = 0$ with a range determined by $b_{ij}$.

For an anion, the short-range interactions with a nearest-neighbour cation *oppose* the dipole induced by the electric field from that cation. To fit the *ab initio* data on halide-ion polarization in alkali halides [26] a value of $c_{-+} = 2.0$ has been used and, with this choice, $b_{ij}$ has been found to scale with the sum of the ionic radii ($\sigma^i$):

$$b_{ij} = \frac{d_{-+}}{\sigma^i + \sigma^j} \tag{2.7}$$

as would be expected from the physical picture of the origin of the short-range effect in the overlap of ionic charge densities. It is not clear that these alkali halide considerations will transfer directly to the $PbF_2$ situation, although similar values might be expected. We have experimented with a range of values for $c_{-+}$ and $b_{-+}$ in the present calculations and find, from a comparison of predicted and experimental phonon frequencies *vide infra*, that values of $c_{-+} = 1.5$ and $b_{-+} = 1.8$ are the most successful (cf. $b_{-+}$ = 1.60 for KF, in which the cation has a similar size to the $Pb^{2+}$ ion).

Much less is known about the short-range polarization of a cation by an anion, although general considerations indicate that, in contrast with the anion–cation situation, it should *enhance* the Coulombic dipole, i.e. that $c_{+-}$ should be negative. For $CaF_2$ various empirical considerations [17,28] indicate that if the range parameter $b_{+-}$ is set equal to that for the anion–cation case, $b_{-+}$, since they refer to the overlap of the same charge densities, then $c_{+-} \sim -0.4$. In the present work we have explored the effect of varying $c_{+-}$ on a variety of properties, whilst keeping all the parameters determined *ab initio* fixed. We will illustrate, to some extent, the way that the polarization effects influence the observable properties below. The optimum value for $c_{+-}$ is $\sim -0.3$, and most of the results below have been obtained with this value.

## 3. Testing the potential

### *3.1. Energy/volume data for fluorite and cotunnite*

Table 3 lists the calculated volumes and energies at the energy minima for both the fluorite and cotunnite structures along with the transition pressure. The experimental data are from [29] in

**Table 3.** Comparison of the model volumes, energetics and transition pressures for the two major forms of $PbF_2$.

| Observable | Experimental | Calculated | Percentage difference |
|---|---|---|---|
| $\beta$-form volume per formula unit | 52.395 Å$^3$ | 51.45 Å$^3$ | 1.8% |
| $\alpha$-form volume per formula unit | 47.74 Å$^3$ | 47.48 Å$^3$ | 0.5% |
| $\beta$-form lattice energy | 2475 kJ mol$^{-1}$ | 2446 kJ mol$^{-1}$ | 1.2% |
| Transition pressure | 0.5 GPa | 3.0 GPa | 500% |

the case of the volumes, and [8] for the lattice energy (calculated from the Born–Haber cycle). Given that no empirical data have been used in the non-polarization part of the potential, this is considered good agreement between the predicted and observed properties of the perfect crystals.

The energy/volume curves are shown in figure 2. The 0 K transition pressure was calculated to be 3 GPa from the common tangent to the two curves. At first sight, the comparison of experimental (0.5 GPa) [2] and calculated transition pressure suggests a serious problem. However, it should be noted that a small increase in the lattice energy of the $\alpha$-form (of order 5 kJ mol$^{-1}$, i.e. 0.2% of the lattice energy) would bring the gradient of the common tangent into agreement with experiment. In fact, our calculation is biased towards the $\beta$-form, as the pair potential is based upon a fit to the energetics of the fluorite phase. Were we to allow for the coordination number dependence of the potential, by using a compressible-ion model (CIM) [20, 30], it is likely that the energy of the $\alpha$-phase would be reduced. In general terms, allowing for ion compressibility stabilizes higher-coordination structures relative to the predictions of a pair potential. For $CaF_2$, for which a CIM was devised, we showed [17] a stabilization of the $\alpha$-phase of the required order to bring the $PbF_2$ data into agreement with experiment. The effects of entropy, ignored in these calculations, may also have an effect on the transition pressure, since the experimental value refers to room temperature.

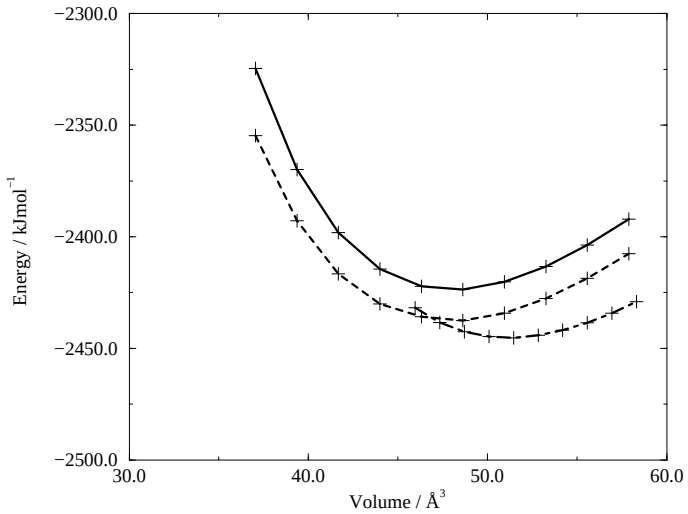


**Figure 2.** Internal energy versus volume curves are shown for the $\alpha$- (cotunnite, or $PbCl_2$ structure; solid line) and $\beta$- (fluorite, or $CaF_2$ structure; dot–dashed line) forms of $PbF_2$, after relaxation of the atomic positions. For the $PbCl_2$ the effect of omitting the cation polarization is illustrated (dashed line).

As remarked previously, polarization effects play no role in the cubic fluorite structure, but they do contribute to the energetics of the $\alpha$-phase, where the site symmetry is lower. They were found to increase the magnitude of the lattice energy of the $\alpha$-form by around 28 kJ mol$^{-1}$ (i.e. around 1%). Cation polarization is responsible for approximately half the energy difference, and in the absence of cation polarization, the transition pressure is calculated to be 13 GPa, which is substantially higher than that calculated when cation polarization is included. We noted in the introduction that the transition pressure for $PbF_2$ is significantly lower than would be expected, on a simple ionic picture of the interactions, from a comparison with the alkaline-earth fluorides. It seems plausible to attribute this to the increased size of the polarization effects in $PbF_2$, associated with the increased cation polarizability.

### *3.2. The $PbF_2$ molecule*

In general, one would not expect an ionic interaction model for condensed phase properties to transfer well to describing the isolated molecule—in the condensed phase the electron density of anions is compressed by an effective potential from the charge densities of neighbouring ions, so the polarizability and ion size are smaller than in the gas phase [19, 31]. Nevertheless, for $CaF_2$ we were able to obtain some useful information about the cation polarization effects from considerations of the properties of the $CaF_2$ *molecule* which has been studied spectroscopically in the gas phase and also in an inert matrix. Within the ionic model, the bending of the F–M–F bond is due to the polarization of the cation, primarily by the charges on the anions, which can occur only when the molecule is bent. A dipole induced on the cation acts to screen the repulsive anion–anion interactions and can lead to a favourable bent configuration. The $CaF_2$ molecule is apparently linear in isolation (though with a very low bending frequency) and bent to about 140° in a matrix, which we were able to reproduce with the ionic model [28]. In $PbF_2$ the observed degree of bending is much greater, ∼98° [32], which is consistent with the much greater polarizability of the $Pb^{2+}$ cation compared to that of $Ca^{2+}$. The energy minimum for the present potential model is not in particularly good agreement with the experimental geometry—the bond angle is too small by about 20% and the bond lengths are too short by about 5%; it would appear that the ion compression effects to which we referred above are too severe in the $PbF_2$ case to allow for the potential to be transferred. However, we can still obtain useful information on the polarization effects by comparing the dipole moment of the molecule with that calculated from the model at the experimentally observed geometry. The self-consistent molecular dipole generated in this configuration was found to be $6.24D$ compared with the experimental value of $5.669D$. The value of $6.24D$ results from the partial cancellation of the dipole due to the ionic charges of $13.71D$ by the induced dipoles, and therefore suggests that the model of the internal charge distribution is well represented by the polarization model. Furthermore, it is to be expected that the cancellation of the ion charge dipole moment by the induced dipoles will be less complete in the calculation than in reality, since in a $PbF_2$ molecule the fluoride 'ion' will be less compressed than in a crystal, and hence the polarizability of the fluoride will be higher in the molecule than the *ab initio* in-crystal value of 7.783 au.

The Hessian of the potential evaluated at the minimum-energy geometry given in reference [32] gives the following vibrational frequencies: 678 cm$^{-1}$ ($A_1$), 565 cm$^{-1}$ ($B_2$) and 148 cm$^{-1}$ ($A_1$). These compare quite well with the experimentally observed values (Ne matrix isolated): 545.7 cm$^{-1}$ ($A_1$), 522.5 cm$^{-1}$ ($A_1$) and 170 cm$^{-1}$ ($A_1$).

### *3.3. Phonon dispersion relationships*

Whilst the static calculations (section 3.1) indicate that the potential works well in the region corresponding to the crystal energy minima, an accurate representation of a dynamical process, such as superionicity, requires the potential to be accurate over a broader range of possible ion configurations. A convenient method for examining the potential for general, distorted condensed phase configurations is to calculate the phonon dispersion relations. Different phonon frequencies correspond to different lattice vibration modes, all of which will involve different relative displacements of the ions. The phonons are particularly sensitive to the polarization effects, whereas, as we have remarked, these have relatively little effect on the properties of the perfect crystals. In fact, comparison of the phonon dispersion curves for $PbF_2$ with those for the alkaline-earth fluorides with the fluorite structure reveals interesting differences. The alkaline-earth systems (e.g. the $CaF_2$, $SrF_2$ and $BaF_2$ data in references [9–11]) all have very similarly structured curves, but the shape of some branches is qualitatively different for $PbF_2$, and we shall show that this is strongly related to the high polarizability of the $Pb^{2+}$ cation.

The phonons are calculated from simulation using the following equations for the longitudinal and transverse currents of the charge, mass and a third variable which picks out the relative motion of $F^-$ ions. The Fourier transforms of the correlation functions of these currents contain peaks which give the phonon frequencies at a particular $\boldsymbol{k}$-vector. The longitudinal correlation function, $C^L_{XX}$, for the variable $X^j$ ($=Q^j$, the charge on ion $j$, for example) is given by

$$C^L_{XX}(\boldsymbol{k},t)=\left\langle\left(\sum_{j=1}^{N}-X^j(t)\mathrm{i}\boldsymbol{k}\cdot\boldsymbol{v}^j(t)\mathrm{e}^{-\mathrm{i}\boldsymbol{k}\cdot\boldsymbol{r}^j(t)}\right)\left(\sum_{l=1}^{N}X^l(t)\mathrm{i}\boldsymbol{k}\cdot\boldsymbol{v}^l(t)\mathrm{e}^{-\mathrm{i}\boldsymbol{k}\cdot\boldsymbol{r}^l(t)}\right)\right\rangle \tag{3.1}$$

whilst the transverse correlation function is given by

$$C^T_{XX}(\boldsymbol{k},t)=\left\langle\left(\sum_{j=1}^{N}-X^j(t)\mathrm{i}\boldsymbol{k}\wedge\boldsymbol{v}^j(t)\mathrm{e}^{-\mathrm{i}\boldsymbol{k}\cdot\boldsymbol{r}^j(t)}\right)\cdot\left(\sum_{l=1}^{N}X^l(t)\mathrm{i}\boldsymbol{k}\wedge\boldsymbol{v}^l(t)\mathrm{e}^{-\mathrm{i}\boldsymbol{k}\cdot\boldsymbol{r}^l(t)}\right)\right\rangle. \tag{3.2}$$

The frequencies at the $\boldsymbol{k}$-vector $\{\xi,0,0\}$, $\{\xi,\xi,0\}$ and $\{\xi,\xi,\xi\}$ symmetry directions can be calculated in the case of a simulation cell based on $4\times4\times4$ unit cells (768 atoms) for $\xi=\frac{1}{4}$, $\frac{1}{2}$, $\frac{3}{4}$ and 1, whilst for $3\times3\times3$ unit cells (324 atoms), the frequencies at points $\xi=\frac{1}{3}$, $\frac{2}{3}$ and 1 can be obtained. With $X^j=Q^j$, the optic mode peak dominates the spectrum, and for $X^j=M^j$ (ion mass) the acoustic branch is dominant. To pick out the second 'optic' branch, $X^j$ is set equal to unity for ions on one of the two fcc sublattices, which together make up the simple cubic lattice of $F^-$ in the fluorite structure, and to minus one for the other sublattice.

Figure 3(a) shows the phonon dispersion curves calculated from a dynamics run of 60 ps at 10 K with a full dipolar PIM with a cation dipole polarization enhancement parameter of $c_{+-}=-0.3$, and the other potential parameters as discussed in section 2. The run was started from a perfect crystal at the experimental density and random velocities selected from a Maxwell–Boltzmann distribution. The experimental curves [3] are shown for comparison. The agreement both in terms of absolute frequency and the shapes of the curves is excellent.

The role of the cation polarization in obtaining this agreement is illustrated by performing a second set of simulations with all potential parameters and ionic masses as above, except that the polarizability of the '$Pb^{2+}$' ion is set to a value of 5.2 au. This is the polarizability of an $Sr^{2+}$ cation which, as we have remarked previously, is the closest in size to a $Pb^{2+}$ cation amongst the alkaline earths. By making this substitution we hope to identify the reasons underlying the qualitative difference of shape of the phonon dispersion curves for the alkaline-earth and lead fluorides which were commented on in the introduction. The resulting phonon dispersion

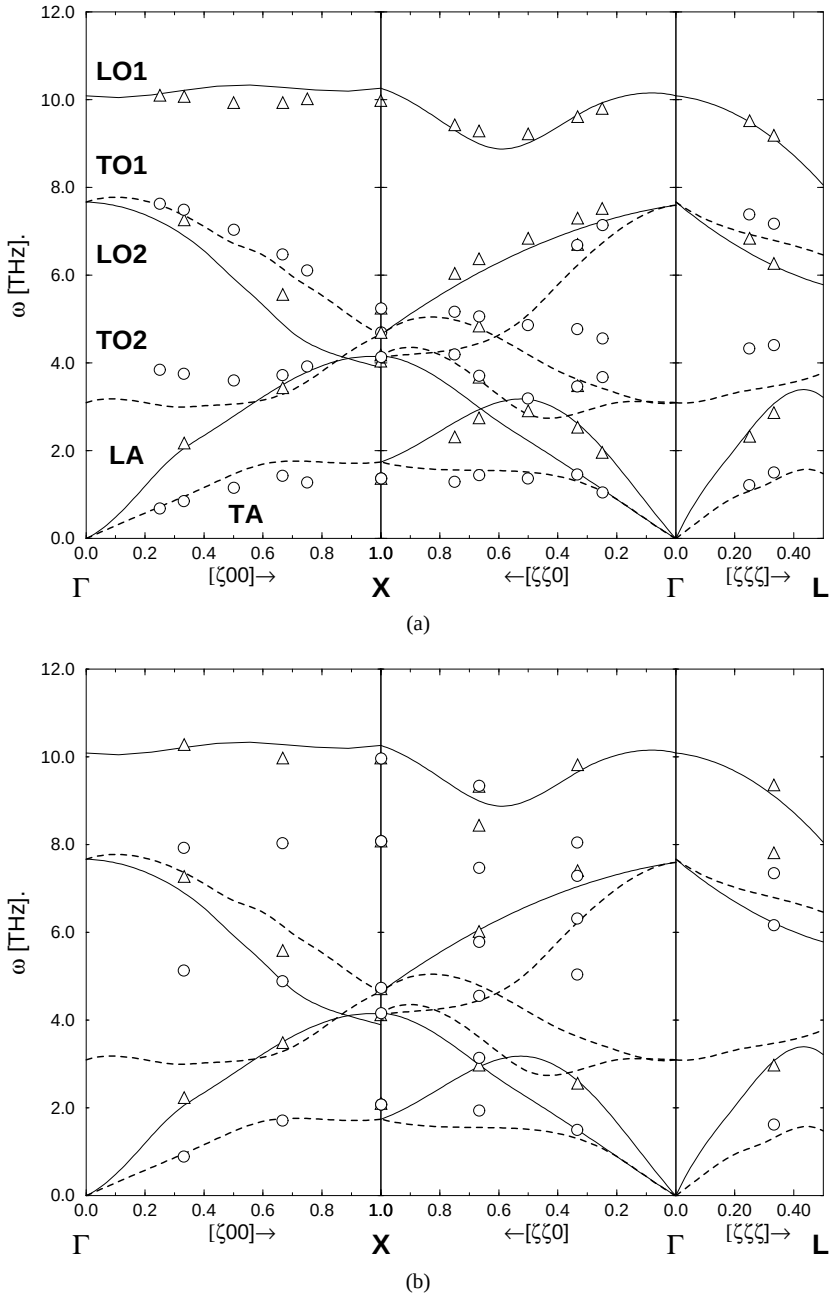


**Figure 3.** Phonon dispersion curves obtained with three different models for the cation polarization are shown and compared with the experimental data for $\beta$-$PbF_2$ (solid lines: longitudinal; dotted lines: transverse). In all cases the triangles represent the simulated longitudinal modes and the circles the transverse. In (a) the dispersion curves calculated with the full model are shown. In (b) the cation polarizability is assigned a value of 5.2 au, which is the value appropriate to a $Sr^{2+}$ ion: note the straightening of the TO1 mode (with respect to (a)) along ($\xi$, 0, 0) *inter alia*. In (c) we show the dispersion curves calculated with the cation polarization enhancement omitted: note the worsening of the agreement with experiment for TO2, in particular.

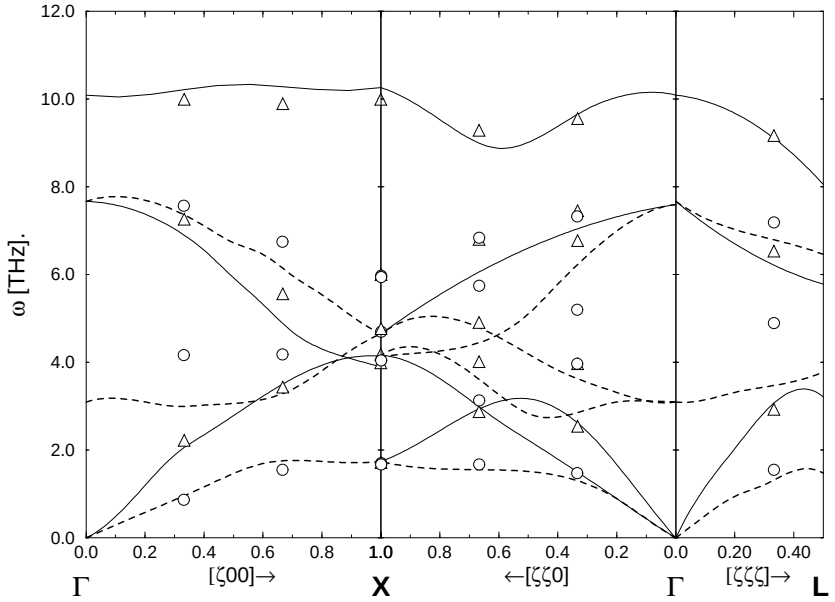


(c)

**Figure 3.** (Continued)

curves are presented in figure 3(b), where they are, again, superimposed on the experimental dispersion curves for $PbF_2$ in order to facilitate comparison with figure 3(a). The calculated phonon dispersion curves with the reduced cation polarizability now show the characteristic features of the alkaline-earth fluorides [9–11]. The TO1 mode now has an almost constant frequency along the (100) direction compared with a significant softening towards the X point seen in $PbF_2$ (figure 3(a)). The TO2 mode is significantly softer at the Γ point in the $PbF_2$ curves. To obtain more quantitative agreement with the $SrF_2$ data, we would have to shift the cation mass, which strongly affects the frequencies of the acoustic modes.

The softening of the TO1(X) and TO2(Γ) modes by the cation polarization can be understood from a consideration of the ionic displacements for these modes. Figure 4 shows the ion motions relating to the two TO modes considered above (TO1(X) and TO2(Γ)) and the LO1(X) mode which remains alkaline-earth-like. Both of the TO modes shown would be heavily influenced by cation polarization effects. In the TO2(Γ) mode, for example, the cation fcc sublattice moves against *both* the anion fcc sublattices resulting in a large electric field on the central cation and hence a large induced dipole for a polarizable cation which acts to soften this mode with respect to the alkaline earths. Conversely, the TO1(Γ) mode (not shown) involves the two anion fcc sublattices moving out of phase leading to much smaller fields at the cation site and so much less significant softening. The LO1(X) mode also remains alkaline-earth-like as the motion involves the symmetric 'breathing' of the anion sublattices about the cation. Indeed, the study of the mode frequencies shows that this mode reduces in frequency slightly as the cation size increases—that is, as the anion sublattice expands slightly.

Finally, in figure 3(c) we show the phonons predicted for $PbF_2$ when the cation polarization enhancement factor $c_{+-}$ is set to zero. It can be seen that there is a worsening in the quality of agreement with experiment relative to figure 3(a) (where $c_{+-} = -0.3$) in the polarization-sensitive branches. Use of a higher (more negative) $c_{+-}$ softens the TA branch too much. Overall we see that by adjustment just of the parameters controlling the short-range polarization

a)

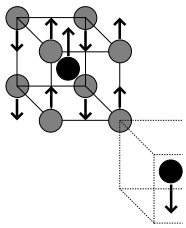

b)

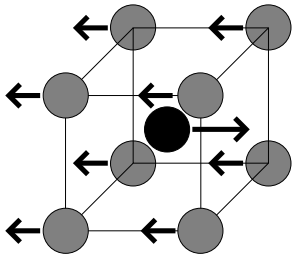

c)

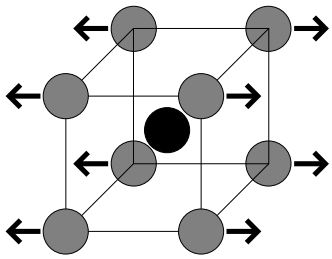

**Figure 4.** The ionic displacements in the normal modes corresponding to certain key points in the phonon dispersion curve, to illustrate the origin of their (in)sensitivity to cation polarization: (a) TO1(X); (b)TO2 (Γ); (c) LO(X).

terms, whilst keeping all other parameters at values where they have been fixed by electronic structure calculations, we obtain good agreement with experiment. The optimal short-range polarization parameter is similar to that found in other systems. Even in the full model, figure 3(a), the TO2 mode is at slightly too high a frequency, whereas all other branches seem to be in good agreement with experiment. This could be remedied by a change in the short-range repulsion between two $F^-$ ions. We have not permitted ourselves this freedom in the pursuit of agreement with the experimental data, as this part of the potential was derived from the *ab initio* calculations.

## 4. The superionic state

### *4.1. Ion diffusion*

Calculations to establish the position of the transition to superionic behaviour were carried out on systems of 324 ions ($3 \times 3 \times 3$ unit cells). A series of runs in which the temperature

was progressively increased was carried out, and the mean square displacements of the ions monitored to detect the onset of diffusion. Each run was of roughly 100 ps duration. The temperature was controlled with a Nosé–Hoover thermostat and the volume of the cell was allowed to change isotropically to maintain constant pressure [33, 34]. An example of the mean square displacements of the ions from the initial configuration of such a run is shown in figure 5. It can be seen that at this temperature (950 K) diffusion of the anions begins shortly after start-up with the ions quickly achieving their mean diffusion rate. The cations, on the other hand, show no diffusion. At lower temperatures anion diffusion commenced only after an appreciable waiting time, which is probably related to the time for the creation of some kind of defect on the anion sublattice. The presence of this waiting time, with its variation from run to run, made the accurate location of a starting temperature for ionic conduction difficult . Starting from an already superionic configuration (obtained from a simulation at higher temperature), superionicity was retained for several thousand MD steps in simulations at temperatures down to 650 K. These results are consistent with a superionic 'transition temperature' in the range 700–950 K, which is higher than reported experimentally [35] by $\sim$250 K. Even at the upper end of this range, the transition temperature is much lower than in the $CaF_2$ calculations [17] under comparable conditions. Much of this lowering is due to the cation polarization. In simulations carried out with unpolarizable cations and otherwise identical potentials and simulation conditions, ion diffusion was not detected until $\sim$1400 K. At these temperatures the polarizable-cation simulations had already melted (at around 1200 K); melting did not occur until much higher temperatures in the unpolarizable-cation case. It would appear that the cation polarization plays an important role in stabilizing the unsymmetrical ionic arrangements associated with the anion diffusion in the crystal, and in the molten state. The temperature for the onset of ion conduction was lowered by an increase in the cation polarization enhancement factor (from $c_{+-} = -0.3$). However, this would worsen other predicted properties, especially the phonon dispersion curves.

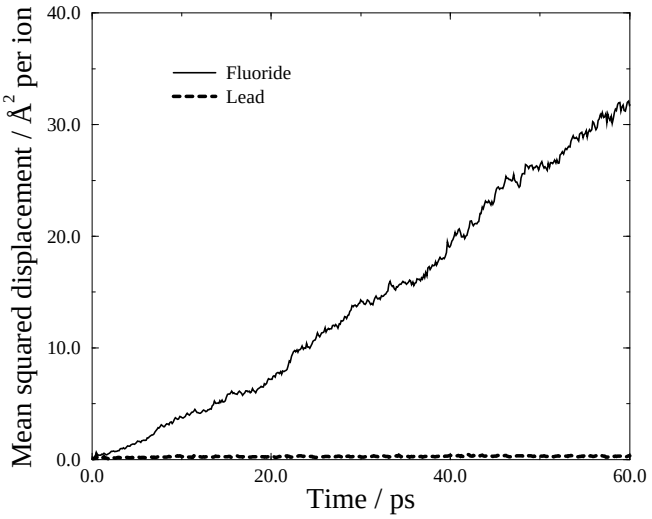


**Figure 5.** The mean anion and cation displacements from the initial configuration during a run at 950 K.

From the slope of the mean square displacement versus time (as in figure 5) a value for the diffusion coefficient may be calculated. At 1000 K, for example, this gives $D = 1.9 \times 10^{-5}$ cm$^2$ s$^{-1}$. If we assume independent ion migration we may estimate a value for the

ionic conductivity of $\sigma = 1.4\,\Omega^{-1}\mathrm{cm}^{-1}$ which is about one-half of the experimental value [35]. This underestimate of the ion mobility is qualitatively consistent with the high value of the transition temperature.

The possibility of superionic conduction in the $\alpha$-phase (cotunnite) was also investigated. At a temperature of 1000 K, where the $\beta$-phase shows appreciable conduction, the diffusion coefficients of cations and anions were zero. This is in agreement with observations of the macroscopic conductivity in the $\alpha$-phase [2]. Recent nmr studies [36] have shown that the $F^-$ ions are involved in some kind of hopping motion in this phase, and that this is promoted by KF doping. However, it would appear that this hopping does not lead to ionic motion on macroscopic length scales, and hence to conduction. A clarification of these apparently contradictory observations is one of the long-term objectives of our study.

### *4.2. Diffuse neutron scattering*

The disorder in the superionic state gives rise to appreciable diffuse scattering and this has been studied using single-crystal neutron scattering for $SrCl_2$ and $CaF_2$, as well as $PbF_2$, by Hutchings *et al* [4]. Intriguingly, the patterns of diffuse scattering are different for the three materials, which suggests that the type of fluoride-ion disorder may be different in each. It is important, therefore to examine the pattern of diffuse scattering predicted in the simulations, and check that it agrees with the pattern found experimentally for $PbF_2$. Contour plots of the diffuse intensity for $PbF_2$ show a broad peak along the [100] direction centred at roughly (2.3, 0, 0) with a second, weaker feature along [111], peaking just beyond (2, 2, 2).

The total neutron scattering intensity is proportional to

$$S^{tot}(\boldsymbol{Q}) = S_{\mathrm{PbPb}}(\boldsymbol{Q}) + 2S_{\mathrm{PbF}}(\boldsymbol{Q}) + S_{\mathrm{FF}}(\boldsymbol{Q}) \tag{4.1}$$

where

$$S_{\alpha\beta} = \langle A^*_\alpha(\boldsymbol{Q}) A_\beta(\boldsymbol{Q})\rangle. \tag{4.2}$$

$A_\alpha(\boldsymbol{Q})$ gives the amplitude of scattering by species $\alpha$ at scattering vector $\boldsymbol{Q}$:

$$A_\alpha(\boldsymbol{Q}) = \sum_{j=1}^{N_\alpha} b^\alpha_{coh} \mathrm{e}^{\mathrm{i}\boldsymbol{Q}\cdot\boldsymbol{r}^j} \tag{4.3}$$

where $b^\alpha_{coh}$ is the value of the scattering length for species $\alpha$. In simulations, periodic boundary conditions are employed, so the only points at which scattering intensity can be calculated must satisfy

$$\boldsymbol{Q} = \frac{2\pi}{na}(l_x, l_y, l_z) \tag{4.4}$$

where $a$ is the unit-cell length of the crystal, $n$ is the number of unit cells along a given direction of the simulation cell, and $l_x$, $l_y$ and $l_z$ are integers. The total scattering contains contributions from the average structure of the system, which is responsible for the Bragg scattering:

$$S^{\mathrm{Bragg}}(\boldsymbol{Q}) = |\langle A_{\mathrm{Pb}}(\boldsymbol{Q}) + A_{\mathrm{F}}(\boldsymbol{Q})\rangle|^2 \tag{4.5}$$

and from diffuse scattering, which is due to thermal and structural disorder:

$$S^{diff}(\boldsymbol{Q}) = S^{tot}(\boldsymbol{Q}) - S^{\mathrm{Bragg}}(\boldsymbol{Q}). \tag{4.6}$$

These quantities were calculated in simulations performed at 1098 K using simulation cells containing $4 \times 4 \times 4$ unit cells. The diffuse scattering intensity distributions along the principal [100], [111] and [110] directions are shown in figure 6. The horizontal axis is labelled by $n$, where $\boldsymbol{Q} = n\hat{\boldsymbol{Q}}$ and $\hat{\boldsymbol{Q}}$ is a base vector for each direction, i.e. $\hat{\boldsymbol{Q}} = (2\pi/a)(1, 0, 0)$,

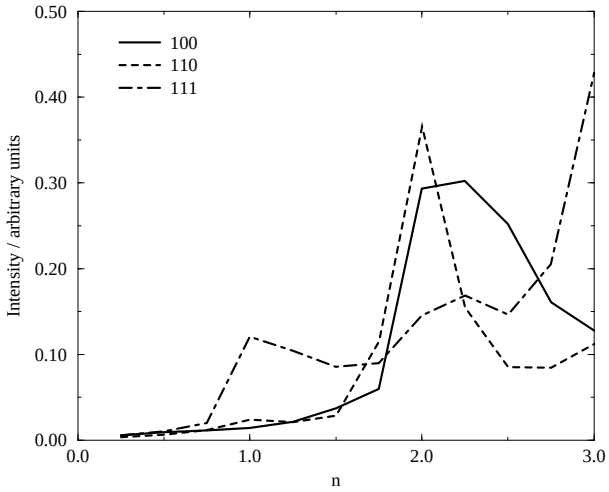


**Figure 6.** Diffuse neutron data calculated along the three principal crystallographic directions at 1098 K, plotted versus the distance along $(2\pi/l, 0, 0)$, $(2\pi/l, 2\pi/l, 0)$ and $(2\pi/l, 2\pi/l, 2\pi/l)$ vectors.

for [100], $\hat{\boldsymbol{Q}} = (2\pi/a)(1, 1, 0)$ for [110] and $\hat{\boldsymbol{Q}} = (2\pi/a)(1, 1, 1)$ for [111]. The thermal diffuse scattering should constitute a background rising as $Q^2$ along each direction. As can be seen, the main areas of additional intensity (away from the Bragg peaks), which is due to the structural disorder, lie in exactly the same regions of $\boldsymbol{Q}$-space as in experiment, i.e. around (2.25, 0, 0) and (2.25, 2.25, 2.25).

A consideration of the real-space structures responsible for these features, their relaxation and their relationship to the superionic conduction process will be given in a future paper. Note that these issues were also addressed in the experimental paper [4].

## 5. Conclusions

The results indicate that the *ab initio* parametrized, formal charge ionic model gives excellent predictions for a range of properties of $PbF_2$. Qualitative differences between $PbF_2$ and alkaline-earth fluorides of similar cation size in properties such as the melting and superionic transition temperature, the transition pressure between the $\beta$- and $\alpha$-forms, and the shapes of the phonon dispersion curves seem to be attributable to the highly polarizable nature of the $Pb^{2+}$ cation. The predicted transition temperature appears to be too high by about 150 K with respect to experiment, though it is possible that improved simulation technique (larger system size) would improve this somewhat.

The pattern of diffuse neutron scattering predicted in the simulations is in good accord with that found experimentally, which opens the way for further examination of the $F^-$-ion disorder and its relationship to the anion diffusion. The fact that the potential should be transferable to mixtures of $PbF_2$ with other fluorides, notably KF, will enable a study of the enhanced diffusion in such mixtures.

## Acknowledgments

We are grateful to Steve Hull, Clare Grey and Nick Pyper for stimulating discussions and for sending data. MW thanks the Royal Society for a fellowship. The work was supported by EPSRC grant GR/L/49369 and NATO grant CRG972228.

## References


[1] Chandra S 1981 *Superionic Solids. Principles and Applications* (Amsterdam: North-Holland)
[2] Hull S and Keen D A 1998 *Phys. Rev.* B **58** 14 837
[3] Dickens M H and Hutchings M T 1978 *J. Phys. C: Solid State Phys.* **11** 461
[4] Hutchings M T, Clausen K, Dickens M H, Hayes W, Kjems J K, Schnabel P G and Smith C 1984 *J. Phys. C: Solid State Phys.* **17** 3903
[5] Hiernaut J P, Hyland G J and Ronchi C 1993 *Int. J. Thermophys.* **14** 259
[6] Stefanovich E V, Shluger A L and Catlow C R A 1994 *Phys. Rev.* B **49** 11 560
[7] Hull S, Berastegui P, Eriksson S G and Gardner N J G 1998 *J. Phys.: Condens. Matter* **10** 8429
[8] Stark J G and Wallace H G 1991 *Chemistry Data Book* 2nd edn (New York: Murray)
[9] Elcombe M M and Pryor A W 1970 *J. Phys. C.: Solid State Phys.* **3** 492
[10] Elcombe M M 1972 *J. Phys. C.: Solid State Phys.* **5** 2702
[11] Hurrell J P and Minkiewicz V J 1970 *Solid State Commun.* **8** 463
[12] Fowler P W and Pyper N C 1985 *Proc. R. Soc.* A **398** 377
[13] Pyper N C 1986 *Phil. Trans. R. Soc.* A **320** 107
[14] Pyper N C 1991 *Adv. Solid State Chem.* **2** 223
[15] Wilson M, Madden P A, Peebles S A and Fowler P W 1996 *Mol. Phys.* **88** 1143
[16] Wilson M and Madden P A 1997 *J. Chem. Soc. Faraday Trans.* **106** 339
[17] Wilson N T, Wilson M, Madden P A and Pyper N C 1996 *J. Chem. Phys.* **105** 11 209
[18] Gillan M J 1995 Private communication
[19] Madden P A and Wilson M 1996 *Chem. Soc. Rev.* **25** 339
[20] Wilson M, Madden P A, Pyper N C and Harding J H 1996 *J. Chem. Phys.* **104** 8068
[21] Bork M and Hoppe R 1996 *Z. Anorg. Allg. Chem.* **622** 1557
[22] Stone A J 1996 *The Theory of Intermolecular Forces* (Oxford: Clarendon)
[23] Walker A B, Dixon M and Gillan M J 1982 *J. Phys. C: Solid State Phys.* **15** 4061
[24] Fowler P W and Madden P A 1985 *Phys. Rev.* B **31** 5443
[25] Mahan G D and Subbaswamy K R 1990 *Local Density Theory of Polarizability* (London: Plenum)
[26] Ẅemmer P, Fowler P W, Wilson M and Madden P A 1999 *J. Chem. Phys.* **111** 2038
[27] Tang K T and Toennies J P 1984 *J. Chem. Phys.* **80** 3726
[28] Sugarman R S, Wilson M and Madden P A 1999 *Chem. Phys. Lett.* **308** 509
[29] Wyckoff R W G 1963 *Crystal Structures* 2nd edn, vol 1 (New York: Interscience)
[30] Rowley A J, Ẅemmer P, Wilson M and Madden P A 1998 *J. Chem. Phys.* **108** 10 209
[31] Wilson M 1997 *J. Phys. Chem.* **101** 4917
[32] Dai D, Al-Zahrani M M and Balasubramanian K 1994 *J. Phys. Chem.* **98** 9233
[33] Allen M P and Tildesley D J 1986 *Computer Simulation of Liquids* (Oxford: Oxford University Press)
[34] Hutchinson F and Madden P A 1999 in preparation
[35] Lorenzana H E, Hepeis J E, Lipp M J, Evans W J, Radousky H B and van Schilfgaarde M 1997 *Phys. Rev.* B **56** 543
[36] Grey C P and Wang F 1995 *J. Am. Chem. Soc.* **117** 6637